KnE Social Sciences

AICoLiN
Academic International Conference on Literacy and Novelty
Volume 2021

Knowledge E
enriching | engaging | empowering

Conference Paper

On Throughput for UAV Relay Assisted for Use in Disaster Communications

Van Vo Nhan[1], Dang Ngoc Cuong[1], Tran Ban Thach[1], and Hung Tran[2]

[1]Duy Tan University, Vietnam
[2]Phenikaa University, Vietnam

ORCID:
Van Vo Nhan: https://orcid.org/0000-0003-0753-5203

Abstract

In this paper, the system performance of an energy harvesting (EH) unmanned aerial vehicle (UAV) system for use in disasters was investigated. The communication protocol was divided into two phases. In the first phase, a UAV relay (UR) harvested energy from a power beacon (PB). In the second phase, a base station (BS) transmitted the signal to the UR using non-orthogonal multiple access (NOMA); then, the UR used its harvested energy from the first phase to transfer the signal to two sensor clusters, i.e., low-priority and high-priority clusters, via the decode-and-forward (DF) technique. A closed-form expression for the throughput of the cluster heads of these clusters was derived to analyze the system performance. Monte Carlo simulations were employed to verify our approach.

Keywords:

Corresponding Author:
Van Vo Nhan

Published: 8 July 2021

Publishing services provided by Knowledge E

Selection and Peer-review under the responsibility of the AICoLiN Conference Committee.

1. Introduction

Recently, unmanned aerial vehicles (UAVs) are considered as promising solutions for numerous applications, such as aerial monitoring, photography, precision agriculture, traffic control, telecommunications, and specially search and rescue [1], [2]. The low-altitude UAVs has attracted massive research attentions in disaster communications due to their mobility, elevated positions, reducing cost, and making them more easily accessible to the surveillance area [3], [4]. For example, the authors in [5] proposed an efficient optimization approach for UAV relay assisted to cope with the network destruction under the natural disaster. Furthermore, N Zhao *et al.* focused on a unified framework for a UAV assisted emergency network in disaster areas. The numerical result shown that the system performance in term of outage probability (OP) of the UAV-assisted emergency network will become higher with larger distance between the base station (BS) and users [6].

Notably, a UAV has a limited amount of energy to maintain its flying and transmission capabilities [6]. Therefore, radio frequency (RF) energy harvesting (EH) techniques are applied to supplement the energy of UAVs for transmission purposes. For example, in [7], a system model with EH at two UAVs is investigated, in which each UAV transmitted signals via power splitting using the energy obtained through EH. Moreover, S Yin *et al.* focused on a cellular network with an energy-constrained UAV relay (UR) and concluded that EH for the UAV could improve the uplink rates achieved via cooperative communication from the UAV to users [8]. In addition, B Ji *et al.* considered a UAV relays' assisted network with EH in order to overcome the large-scale fading between the BS and users. Accordingly, the throughput and delay limited state of the UR were analyzed. The numerical results showed that the UR selection could effectively improve the throughput and reduce the OP of the considered system [9].

Furthermore, non-orthogonal multiple access (NOMA) technique is designed to reuse the resource and increase sharing between the users. For instance, an integrated wireless communication system using NOMA techniques is considered in [10]. A closed-form expression for the OP was derived to evaluate the system performance. The numerical results showed that the system performance achieved with the NOMA scheme was higher than that with orthogonal multiple access (OMA) scheme. Therefore, the combination a UAV and NOMA technique is capable of improving the throughput. For example, P K Sharma *et al.* investigated a UAV to communicate with two users using NOMA and focused on their OP [11]. While M F Sohail *et al.* considered a UAV system applying NOMA technique that optimizes power allocation and UAV altitude to maximize sum-rate for two users [12]. However, the above works have not studied the system performance for the EH UAV relay network in disasters using NOMA technique under imperfect channel state information (CSI). Thus, in this paper, the throughput of the EH UAV relay network is investigated. The primary contributions of this paper are summarized as follows:

- We investigate a UR that forwards the control signal from a BS to two sensor clusters under imperfect CSI and Nakagami-m fading for a disaster scenario.
- We derive the closed-form expression for the throughput of two cluster heads to evaluate the system performance.
- We conduct exhaustive simulations to verify the mathematical analysis and analyze the impact of the parameters (e.g., EH time, the UR's altitude, and the transmit power of the power beacon (PB)) on the system performance.

The remainder of this paper is organized as follows. In Section 2, the system model, communication protocol, and end-to-end signal-to-interference-plus-noise ratio (SINR) are introduced. The throughput of the cluster heads of the low-priority and high-priority clusters are analyzed in Section 3. In Section 4, numerical results are reported and discussed. Finally, conclusions are presented in Section 5.

System model and communication protocol

In this section, we introduce the system model, channel assumptions, communication protocol, and scheduling schemes.

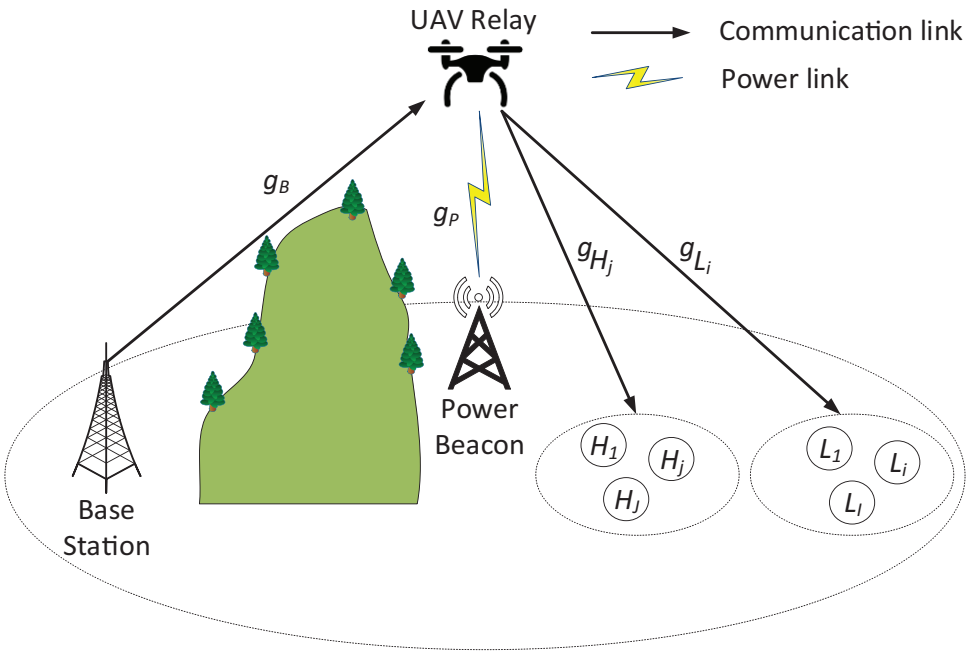

Figure 1: Illustration for the UAV of the relaying system.

1.1. System model and channel assumptions

We investigate a UAV relay assisted emergency networks in disaster area as in Fig. 1. Here, a BS (denoted by B) transmits the signal to multiple sensor nodes (SNs) with the help of a UR (denoted by R). Note that the SNs are grouped based on the quality of service into two sensor clusters, i.e., low-priority cluster (denoted by $L = \{L_1, \cdots, L_I\}$) and high-priority cluster (denoted by $H = \{H_1, \cdots, H_J\}$) to employ NOMA technique for improving the throughput of the considered network [10]. Here, a PB (denoted by P, e.g., radio tower or TV broadcast) exists to transmit a dedicated RF signal to the UR for EH purposes [13]. Without loss of generality, it is assumed that the BS, PB, SNs,

and UR are equipped with a single antenna. The channel coefficients of the B-to-R, P-to-R, R-to-L_i, and R-to-H_j communication links are denoted by g_B, g_P, g_{L_i}, and g_{H_j}, respectively; where $i \in \{1, \cdots, I\}$ and $j \in \{1, \cdots, J\}$.

According to the system model, air-to-ground (A2G) and ground-to-air (G2A) are introduced and assumed that all channels are mutually independent [4]. Here, we set the 3-D coordinate $B(0,0,0)$, $R\left(x_R, y_R, z_R\right)$, $P\left(x_P, y_P, 0\right)$, $R\left(x_{L_i}, y_{L_i}, 0\right)$, and $R\left(x_{H_j}, y_{H_j}, 0\right)$. Furthermore, the A2G path-loss model for the absolute value is given by

$$\bar{\Lambda}_\chi = \phi_\chi d_\chi^{\theta_\chi} \tag{1}$$

where $\chi \in \{B, P, L_i, H_j\}$; θ_χ is the path-loss exponent; the component ϕ_χ is formulated as [14]-[16]

$$\phi_\chi = 10^{c+d} \tag{2}$$

where c and d are defined as

$$c = \frac{10 \log_{10} (4\pi f/c)^2 + \Omega_{NLoS}}{10} \tag{3}$$

$$d = \frac{\Omega_{LoS} - \Omega_{NLoS}}{10 + 10\phi \exp\left[-a\left(\frac{180}{\pi}\delta_\chi - b\right)\right]} \tag{4}$$

where δ_χ is the UAV elevation angle of χ; a and b are constants which depend on the environment (rural, urban, or dense urban) [12]; and Ω_{LoS} and Ω_{NLoS} are environment and frequency dependent parameters such that Ω_{LoS} and Ω_{NLoS} are the excessive path-losses of the light-of-sight (LoS) and non-light-of-sight (NLoS) links owing to shadow fades, respectively [12]. Furthermore, the distances d_χ are obtained as follows:

$$d_B = \sqrt{\left(x_R - x_B\right)^2 + \left(y_R - y_B\right)^2 + z_R^2} \tag{5}$$

$$d_P = \sqrt{\left(x_R - x_P\right)^2 + \left(y_R - y_P\right)^2 + z_R^2} \tag{6}$$

$$d_{L_i} = \sqrt{\left(x_R - x_{L_i}\right)^2 + \left(y_R - y_{L_i}\right)^2 + z_R^2} \tag{7}$$

$$d_{H_j} = \sqrt{\left(x_R - x_{H_j}\right)^2 + \left(y_R - y_{H_j}\right)^2 + z_R^2} \tag{8}$$

Moreover, the imperfect CSI of the A2G and G2A links are considered, i.e., $g_\chi = \hat{g}_\chi + e_\chi$; where $\hat{g}_\chi$ is the channel coefficients estimated by using minimum mean square error for g_χ; and $e_\chi \sim \text{CN}\left(0, \lambda_e\right)$ with λ_e is the channel estimation error and $\text{CN}\left(0, \lambda_e\right)$ is a

scalar complex Gaussian distribution with zero mean and variance λ_e [17]. In addition, we also assume that the channel gains are modeled as Nakagami-m fading with fading severity parameter m_χ [7], i.e., the channel gains are random variables (RVs) distributed following a Gamma distribution. Thus, the cumulative distribution function of channel gain $\left|\hat{g}_\chi\right|^2$ is formulated as follows [9]:

$$F_{\left|\hat{g}_\chi\right|^2}(x) = 1 - \sum_{j=0}^{m_\chi - 1} \left(\frac{m_\chi x}{\Omega_\chi}\right)^j \frac{1}{j!} \exp\left(-\frac{m_\chi x}{\Omega_\chi}\right) \tag{9}$$

where g_χ is a RV with a mean value $\Omega_\chi = \mathrm{E}\left[\left|g_\chi\right|^2\right]$ and $\Gamma(\cdot)$ is the Gamma function.

1.2. Communication protocol

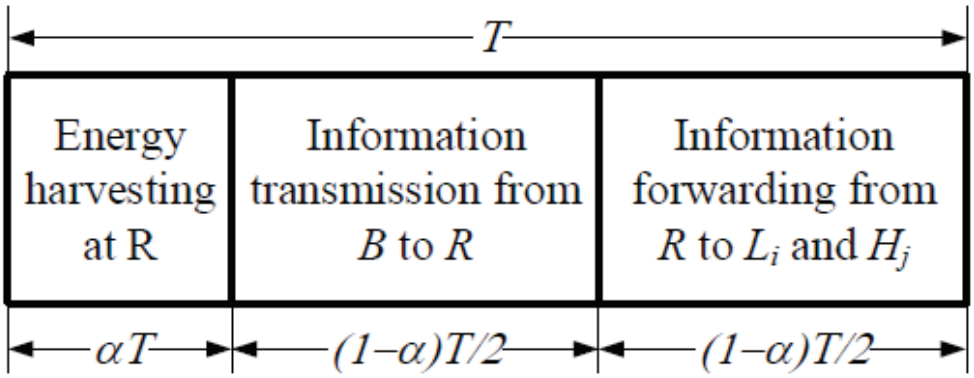

Figure 2: The communication protocol using time splitting for EH and information processing.

The communication protocol is employed for a block time T with two phases as follows (shown in Fig. 2):

- In the first phase, i.e., αT, the UR harvests energy from the PB to prolong its lifetime by using wireless power transfer technique [13], [18], [19]. Therefore, the EH at the UR from the PB can be formulated as [13]

$$E_R = \phi_R \alpha T \mathrm{P}_P \frac{\left|g_P\right|^2}{\bar{\Lambda}_P} \tag{10}$$

where α is EH time fraction, ϕ_R is the energy conversion efficiencies of the R, and P_P is the transmit power of the PB. Therefore, the expected EH at the UR by averaging over the power fading coefficients is as follows [20]:

$$E_R = \phi_R \alpha T \mathrm{P}_P \frac{\lambda_P}{\bar{\Lambda}_P} \tag{11}$$

- In the second phase, the remaining time duration is divided into two equal time slots as $(1-\alpha)T/2$:

- In the first time slot, the BS transmits a superimposed mixed signal $x_B = \sqrt{\mu_{L_i}} x_{L_i} + \sqrt{\mu_{H_j}} x_{H_j}$; where x_{L_i} and x_{H_j} are the signals received by low-priority cluster and high-priority cluster; and μ_{L_i} and μ_{H_j} are the power allocation coefficients that satisfy the condition $\mu_{L_i} + \mu_{H_j} = 1$ and $\mu_{L_j} > \mu_{H_i}$ [17]. Therefore, the received signal at the UR is expressed as

$$y_R = \sqrt{\frac{\mathrm{P}_B}{\bar{\Lambda}_B}} x_B g_B + n_R \tag{12}$$

where $n_R \sim \mathrm{CN}\left(0, N_0\right)$, N_0 is additive white Gaussian noise and P_B is the transmit power of the BS. After receiving the superimposed mixed signal, R applies the NOMA technique to decode x_{L_i} by treating x_{H_j} as the noise. Then, this UR removes x_{L_i} to obtain x_{H_j} by adopting the successive interference cancellation method [17]. Therefore, the instantaneous SINR at the R_1 for detecting x_{F_j} and x_{N_i} from the BS can be written as

$$\gamma_R^{x_{L_i}} = \frac{\mu_{L_i} P_B \left|g_B\right|^2}{\bar{\Lambda}_B \left(\frac{\mu_{H_j} P_B |g_B|^2}{\bar{\Lambda}_B} + P_B \lambda_e + N_0\right)} \tag{13}$$

$$\gamma_R^{x_{H_j}} = \frac{\mu_{H_j} P_B \left|g_B\right|^2}{\bar{\Lambda}_B \left(P_B \lambda_e + N_0\right)} \tag{14}$$

- In the second time slot, the selected i-th and j-th SNs are performed NOMA transmission. Furthermore, R_2 uses its harvested energy to forward the control signal to the SNs using decode-and-forward (DF) protocol; thus, the received signal at D can be formulated as

$$y_{L_i} = \sqrt{\frac{P_R}{\bar{\Lambda}_{L_i}}} x_B g_{L_i} + n_{L_i} \tag{15}$$

$$y_{H_j} = \sqrt{\frac{P_R}{\bar{\Lambda}_{H_j}}} x_B g_{H_j} + n_{H_j} \tag{16}$$

where $n_{L_i}, n_{H_j} \sim \mathrm{CN}\left(0, N_0\right)$ and $\mathrm{P}_R = \frac{E_R}{(1-\tau)T/2}$. Therefore, the selected SNs detect their messages by using NOMA similar to the UR in the first time slot. Consequently, the SINRs for detecting x_{L_i} and x_{H_j} at L_i and H_j are formulated, respectively, as

$$\gamma_{L_i}^{x_{L_i}} = \frac{\mu_{L_i} P_R \left|g_{L_i}\right|^2}{\bar{\Lambda}_{L_i} \left(\frac{\mu_{H_j} P_R |g_{L_i}|^2}{\bar{\Lambda}_{L_i}} + P_R \lambda_e + N_0\right)} \tag{17}$$

$$\gamma_{H_j}^{x_{H_j}} = \frac{\mu_{H_j} P_R \left|g_{H_j}\right|^2}{\bar{\Lambda}_{H_j}\left(P_R \lambda_e + N_0\right)} \tag{18}$$

Moreover, because of the DF strategy, the end-to-end SINRs at i-th and j-th SNs can be written as

$$\gamma_{e2e}^{x_{L_i}} = \min\left\{\gamma_R^{x_{L_i}}, \gamma_{L_i}^{x_{L_i}}\right\} \tag{19}$$

$$\gamma_{e2e}^{x_{H_j}} = \min\left\{\gamma_R^{x_{H_j}}, \gamma_{H_j}^{x_{H_j}}\right\} \tag{20}$$

2. Performance Analysis

2.1. Outage probability

The OP is defined as the end-to-end SINR at the SN that is below a certain outage threshold ($\gamma_{th}^{x_{L_i}}$ or $\gamma_{th}^{x_{H_j}}$), i.e.,

$$O_{L_i} = \Pr\left\{C^{x_{L_i}} < \gamma_{th}^{x_{L_i}}\right\} \tag{21}$$

$$O_{H_j} = \Pr\left\{C^{x_{H_j}} < \gamma_{th}^{x_{H_j}}\right\} \tag{22}$$

where $C^{x_{L_i}}$ and $C^{x_{H_j}}$ are the channel capacity from the BS to L_i and H_j as follows:

$$C^{x_{L_i}} = \frac{1-\alpha}{2} W \log_2\left(1 + \gamma_{e2e}^{x_{L_i}}\right) \tag{23}$$

$$C^{x_{H_j}} = \frac{1-\alpha}{2} W \log_2\left(1 + \gamma_{e2e}^{x_{H_j}}\right) \tag{24}$$

where W is the system bandwidth. In order to improve the system performance, two cluster heads of the two clusters are selected based on the best channel gain from the UR to SNs of the low-priority and high-priority cluster, i.e.,

$$i^* = \arg\max_{1\le i\le I}\left\{\left|g_{L_i}\right|^2\right\} \tag{25}$$

$$j^* = \arg\max_{1\le j\le J}\left\{\left|g_{H_j}\right|^2\right\} \tag{26}$$

Substituting (19) and (23) into (21), we have

$$O_{L_{i*}} = 1 - \underbrace{\Pr\left\{\gamma_R^{x_{L_i}} \ge \Omega_{th}^{x_{L_i}}\right\}}_{A_1} \times \underbrace{\Pr\left\{\gamma_{L_{i*}}^{x_{L_i}} \ge \Omega_{th}^{x_{L_i}}\right\}}_{A_2} \tag{27}$$

where $\Omega_{th}^{x_{L_i}} = 2^{\frac{2\gamma_{th}^{x_{L_i}}}{(1-\alpha)W}} - 1$.

Next, substituting (13) into (27) and after some mathematical manipulations, the term A_1 is given by

$$A_1 = 1 - \sum_{a_1=0}^{m_B-1} \left(\Delta_1\right)^{a_1} \frac{1}{a_1!} \exp\left(-\Delta_1\right) \tag{28}$$

where $\rho_B = \mathrm{P}_B/N_0$ and Δ_1 is defined as

$$\Delta_1 = \frac{m_B \Omega_{th}^{x_{L_i}} \bar{\Lambda}_B \left(\rho_B \lambda_e + 1\right)}{\Omega_B \left(\mu_{L_i} - \Omega_{th}^{x_{L_i}} \mu_{H_j}\right) \rho_B} \tag{29}$$

Similarly, the probability A_2 can be obtained as follows:

$$A_2 = 1 - \prod_{i=1}^{I} \left[1 - \sum_{a_2=0}^{m_{L_i}-1} \left(\Delta_2\right)^{a_2} \frac{1}{a_2!} \exp\left(-\Delta_2\right)\right] \tag{30}$$

where $\rho_R = \mathrm{P}_R/N_0$ and Δ_2 is defined as

$$\Delta_2 = \frac{m_{L_i} \Omega_{th}^{x_{L_i}} \bar{\Lambda}_{L_i} \left(\rho_R \lambda_e + 1\right)}{\Omega_{L_i} \left(\mu_{L_i} - \Omega_{th}^{x_{L_i}} \mu_{H_j}\right) \rho_R} \tag{31}$$

Furthermore, the OP of the cluster head of the high-priority cluster can be derived by the same approach with $O_{L_{i^*}}$ as follows:

$$O_{H_{j^*}} = 1 - B_1 \times B_2 \tag{32}$$

where B_1 and B_2 are defined as

$$B_1 = 1 - \sum_{b_1=0}^{m_B-1} \left(\Pi_1\right)^{b_1} \frac{1}{b_1!} \exp\left(-\Pi_1\right) \tag{33}$$

$$\Pi_1 = \frac{m_B \Omega_{th}^{x_{H_j}} \bar{\Lambda}_B \left(\rho_B \lambda_e + 1\right)}{\Omega_B \mu_{H_j} \rho_B} \tag{34}$$

$$B_2 = 1 - \prod_{j=1}^{J} \left[1 - \sum_{b_2=0}^{m_{H_j}-1} \left(\Pi_2\right)^{b_2} \frac{1}{b_2!} \exp\left(-\Pi_2\right)\right] \tag{35}$$

$$\Pi_2 = \frac{m_{H_j} \Omega_{th}^{x_{H_j}} \bar{\Lambda}_{H_j} \left(\rho_B \lambda_e + 1\right)}{\Omega_{H_j} \mu_{H_j} \rho_R} \tag{36}$$

2.2. Throughput

According to [21], the throughput of the low-priority and high-priority SNs are expressed as follows:

$$\mathsf{T}_{L_{i^*}} = \left(1 - O_{L_{i^*}}\right) \gamma_{th}^{x_{L_i}} \tag{37}$$

$$\mathsf{T}_{H_{j^*}} = \left(1 - O_{H_{j^*}}\right) \gamma_{th}^{x_{H_j}} \tag{38}$$

2.2.1. Numerical Results

In this section, numerical results are provided for evaluating the throughput of the UAV relay in the disaster area. In particular, we consider the effect of the UR's altitudes, the EH time, the channel estimation error on the throughput (in bits/sec/Hz) for the low-priority and high-priority SNs. Unless otherwise stated, the analysis and simulation employ the same system parameters as follows [17]: the carrier frequency $f_c = 2$ GHz; the fading parameters $m_B = m_{L_i} = m_{H_j} = 2$; the EH efficiency coefficient $\phi_R = 0.8$; the EH time fraction $\alpha \in (0, 1)$, $\rho_B, \rho_P \in [0, 20]$ (dB); the coordinates $B(0, 0, 0)$, $P(5, 5, 0)$, $L_i(7, 7, 0)$, $H_j(6, 6, 0)$, $R\left(5, 4, z_R\right)$, where $z_R \in [1, 15]$; the system bandwidth $W = 100$ MHz; the outage thresholds $\gamma_{th}^{x_{L_i}} = 10$ and $\gamma_{th}^{x_{H_j}} = 10$. Furthermore, we investigate the case in which the considered system operates in an urban environment with parameters $a = 9.6177$, $b = 0.1581$, $\Omega_{\text{LoS}} = 1$, and $\Omega_{\text{NLoS}} = 20$.

From Figs. 3 to 5, we can observe that the analytical curves are in excellent agreement with the scatter of Monte Carlo simulations, i.e., the accuracy of our analysis is verified. In particular, Fig. 3 presents the effect of the UR's altitude and the number of the SNs on the throughput. We can see that the throughput of the low-priority and high-priority cluster heads increases as z_R increases. Then, once z_R achieves a certain point, the throughput decreases. This is because when the UAV's altitude is low, the probability of the LoS is low, while the probability of the NLoS is high; however, the high z_R leads to the high path-loss. Therefore, there exists a certain point that achieves the optimal throughput. In addition, the throughput is improved by increasing the number of the SNs due to the higher diversity gain at the SNs.

Fig. 4 shows the impact of the transmit SNR at the PB and channel estimation error on the throughput. We can see that the throughput of the SNs is improved as the transmit power of the PB increases. It is obvious because the high ρ_P leads to high amount of EH at the UR. Moreover, throughput of the SNs decreases when λ_e increases. This is due to that the higher λ_e makes more interferences for decoding the signals at the SNs.

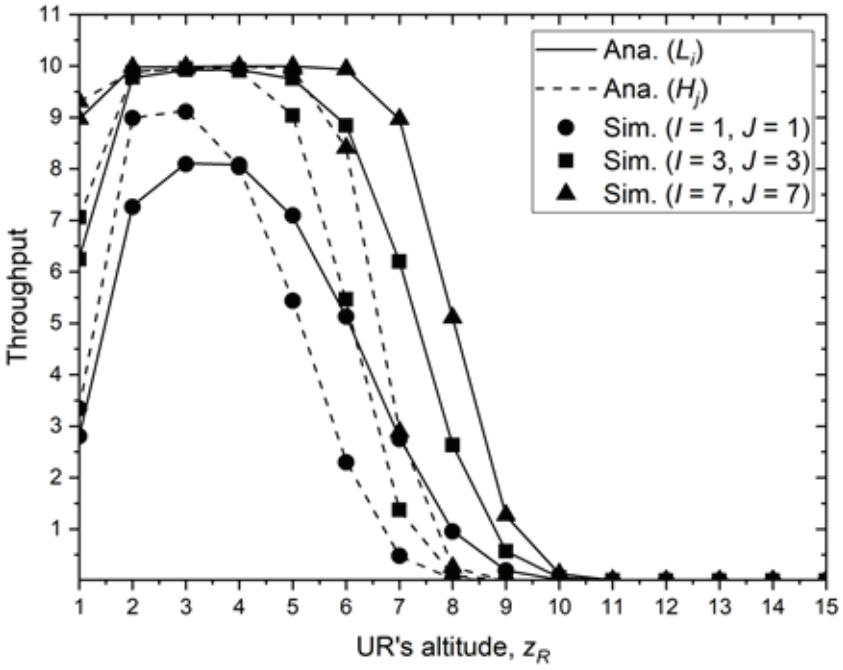

Figure 3: The impact of the UR's altitude and the number of the SNs on the throughput.

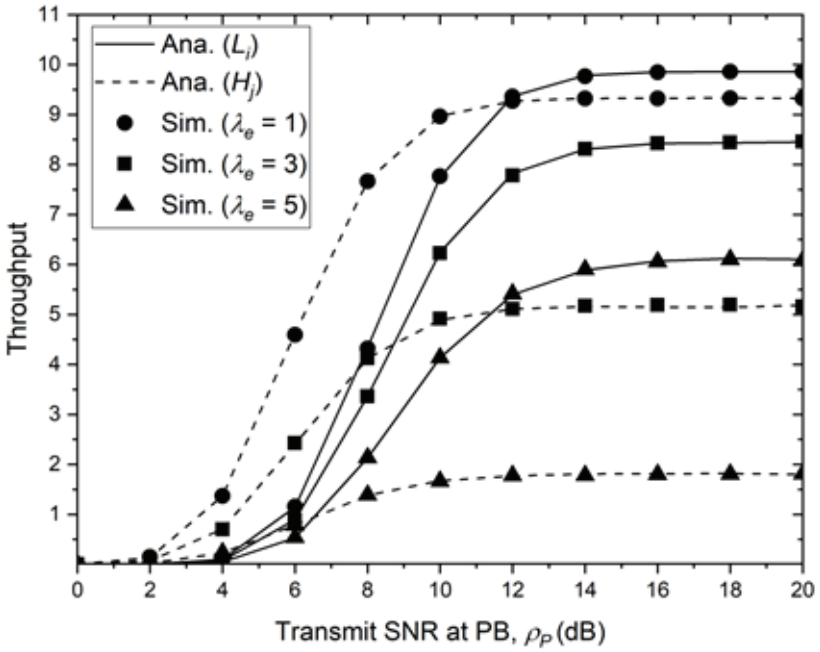

Figure 4: The impact of the transmit SNR at the PB and channel estimation error on the throughput.

Fig. 5 illustrates the impact of the EH time at the UR and channel estimation error on the throughput. It is observed that the throughput increases as α increase and then decreases as α is large. This is because when the EH time is low, the UR harvests little

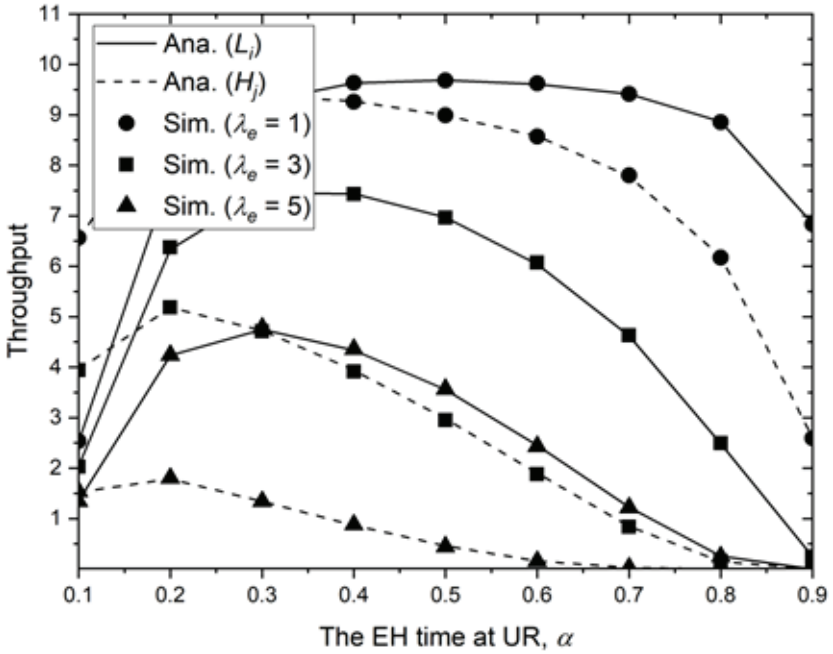

Figure 5: The impact of the EH time at the UR and channel estimation error on the throughput.

energy; while the EH time is large, the remaining time is not enough for information process. Furthermore, similar to Fig. 4, the throughput is improved as the channel estimation error is small.

3. Conclusions

This paper has studied the system performance in terms of throughput of an EH UAV network in a disaster area using NOMA technique. In which, the UR harvests energy from the PB to forward the signal from the BS to the SNs. Accordingly, a closed-form expression for the throughput of the cluster heads of the low-priority and high-priority clusters has been derived under imperfect CSI. Finally, the theoretical analyses of the throughput have been validated by Monte Carlo simulation results. The numerical results showed that there exist the optimal UAV altitude and EH time to maximize the system performance.

References

[1] Zeng Y, Wu Q, Zhang R. Accessing from the sky: a tutorial on UAV communications for 5G and beyond. Proceedings of the IEEE. 2019;107(12):2327–2375.

[2] Sun X, Ng DWK, Ding Z, Xu Y, Zhong Z. Physical layer security in UAV systems: challenges and opportunities. IEEE Wireless Communications. 2019;26(5):40–47.

[3] Zhu Y, Zheng G, Fitch M. Secrecy rate analysis of UAV-enabled mmwave networks using matern hardcore point processes. IEEE Journal on Selelected Areas in Communication. 2018;3(7):1397–1409.

[4] Tang J, Chen G, Coon J. Secrecy performance analysis of wireless communications in the presence of UAV jammer and randomly located UAV eavesdroppers. IEEE Transactions on Information Forensics and Security. 2019;14(11):3026–3041.

[5] Duong TQ, Nguyen LD, Tuan HD, Hanzo L. Learning-aided realtime performance optimisation of cognitive UAV-assisted disaster communication. Global Telecommunications Conference; 2019 Dec 9 -13; Hawaii: IEEE.

[6] Zhao N, Lu W, Sheng M, Chen Y, Tang J, Yu FR, Wong KK. UAV-assisted emergency networks in disasters. IEEE Wireless Communications. 2019;1:45–51.

[7] Ji B, Li Y, Zhou B, Li C, Song K, Wen H. Performance analysis of UAV relay assisted IoT communication network enhanced with energy harvesting. IEEE Access. 2019;7:38738–38747.

[8] Yin S, Qu Z, Li L. Uplink resource allocation in cellular networks with energy-constrained UAV relay. 87th VehicularTechnology Conference; 2018 Jun, 3-6; Porto, Portugal. IEEE.

[9] Ji B, Li Y, Chen S, Han C, Li C, Wen H. Secrecy outage analysis of UAV assisted relay and antenna selection for cognitive network under Nakagami-*m* channel. IEEE Transactions on Cognitive Communication And Networking. 2020;7:1–11.

[10] Guo C, Zhao L, Feng C, Ding Z, Chen H. Energy harvesting enabled NOMA systems with full-duplex relaying. IEEE Transactions on Vehicular Technology.2019;68(7):7179–7183.

[11] Sharma PK, Kim DI. UAV-enabled downlink wireless system with non-orthogonal multiple access. 2017 Globecom Workshops; 2017 December 4-8; Singapore: IEEE. doi: 10.1109/GLOCOMW.2017.8269066.

[12] Sohail MF, Leow CY, Won S. Non-orthogonal multiple access for unmanned aerial vehicle assisted communication. IEEE Access. 2018;6:22716–22727.

[13] Tedeschi P, Sciancalepore S, Pietro RD. Security in energy harvesting networks: a survey of current solutions and research challenges. *IEEE Communications Surveys & Tutorials*, vol. 22, no. 4, pp. 2658-2693, Fourthquarter 2020, doi: 10.1109/COMST.2020.3017665.

[14] Chen Y, Zhao N, Alouini ZDMS. Multiple UAVs as relays: multi-hop single link versus multiple dual-hop links. IEEE Transactions on Wireless Communication, 2018;17(9):6348–6359.

[15] Li Y, Zhang R, Zhang J, Gao S, Yang L. Cooperative jamming for secure UAV communications with partial eavesdropper information. IEEE Access. 2019;7: 94593–94603.

[16] Mozaffari M, Saad W, Bennis M, Debbah M. Unmanned aerial vehicle with underlaid device-to-device communications: performance and tradeoffs. IEEE Transactions on Wireless Communication, 2016;15(6):3949–3963.

[17] Vo VN, So-In C, Tran DD, Tran H. Optimal system performance in multihop energy harvesting WSNs using cooperative NOMA and friendly jammers. IEEE Access. 2019;7:125494–125510.

[18] Nguyen MN, Nguyen LD, Duong TQ, Tuan HD. Realtime optimal resource allocation for embedded UAV communication systems. *IEEE Wireless Communications Letters,* 2019;8(1):225–228.

[19] Vo VN, Nguyen TG, So-In D, Tran H. Outage performance analysis of energy harvesting wireless sensor networks for NOMA transmissions. Mobile Networks and Applications. 2020;25:23–41.

[20] Tran H, Quach TX, Tran H, Uhlemann E. Optimal energy harvesting time and transmit power in cognitive radio network under joint constraints of primary users and eavesdroppers. International Symposium on Personal, Indoor and Mobile Radio Communication;2017 Oct 8-13; Montreal: IEEE.

[21] Mohjazi L, Muhaidat S, Dianati M, Al-Qutayri M. Outage probability and throughput of SWIPT relay networks with differential modulation. 86th Vehicular Technology Conference; 2018 September 24-27; Toronto, Canada: IEEE.